International Journal of Thermal Sciences 48 (2009) 2237–2248

Contents lists available at ScienceDirect

International Journal of Thermal Sciences

journal homepage: www.elsevier.com/locate/ijts

Film cooling effectiveness: Comparison of adiabatic and conjugate heat transfer CFD models

Mahmood Silieti [a], Alain J. Kassab [a,*], Eduardo Divo [b]

[a] Mechanical, Materials, and Aerospace Engineering Department, University of Central Florida, Orlando, FL 32816-2450, United States
[b] Department of Engineering Technology, University of Central Florida, Orlando, FL 32816-2450, United States

ARTICLE INFO

Article history:
Received 18 September 2008
Received in revised form
9 April 2009
Accepted 10 April 2009
Available online 26 May 2009

Keywords:
Conjugate heat transfer
Film cooling
Film cooling effectiveness
Turbulence modeling

ABSTRACT

This paper documents a computational investigation of the film cooling effectiveness of a 3-D gas turbine endwall with one fan-shaped cooling hole. The simulations were performed for adiabatic and conjugate heat transfer models. Turbulence closure was investigated using three different turbulence models: the realizable k–ϵ model, the SST k–ω model, as well as the v^2–f turbulence model. Results were obtained for a blowing ratio of one, and a coolant-to-mainflow temperature ratio of 0.54. The simulations used a dense, high quality, O-type, hexahedral grid with three different schemes of meshing for the cooling hole: hexahedral-, hybrid-, and tetrahedral-topology grid. The computed flow/temperature fields are presented, in addition to local, two-dimensional distribution of film cooling effectiveness for the adiabatic and conjugate cases. Results are compared to experimental data in terms of centerline film cooling effectiveness downstream cooling-hole, the predictions with realizable k–ϵ turbulence model exhibited the best agreement especially in the region for ($2 \leq x/D \leq 6$). Also, the results show the effect of the conjugate heat transfer on the temperature (effectiveness) field in the film cooling hole region and, thus, the additional heating up of the cooling jet itself.

1. Introduction and literature review

Land-based industrial gas turbines are commonly operated continuously over long operational hours. This places severe demands on component life and overall performance for such engines. Increasing performance and efficiency are somewhat conflicting goals as high efficiency requires increasingly elevated turbine inlet temperatures, while increasing turbine inlet temperature reduces component life. Consequently, cooling of gas turbine components is required, and film cooling [1] is widely used as an effective means to maintain component temperatures at acceptable levels. The efficacy of such a cooling scheme can be expressed in terms of cooling effectiveness, which is closely related to the velocity and temperature profiles as well as velocity and thermal boundary layer thickness.

It is well known that significant improvement can be achieved in cooling characteristics of the film by using cooling holes with appropriately designed expanded exits. Goldstein et al. [2] were among the first to pioneer the use of shaped film holes for improved film cooling performance. The performance of inclined holes with 10° laterally flared exit was compared with the performance of streamwise inclined cylindrical film holes. Effectiveness data showed that the shaped film hole provides better lateral coverage and better centerline effectiveness. Makki and Jakubowski [3] presented downstream heat transfer results for a film hole with a trapezoidal shaped expansion. They showed that the shaped film hole consistently provided better heat transfer characteristics than simple cylindrical holes with the same metering section. Also, Makki and Jakubowski reported that the shaped holes offered up to 23% better film cooling performance than the corresponding cylindrical hole.

Schmidt et al. [4] and Sen et al. [5] presented two companion papers in which the effect of adding a 15° forward diffusion exit to a streamwise oriented hole was investigated. They found that the exit diffused film hole demonstrated better spread of adiabatic effectiveness than the cylindrical counterpart. From the heat transfer coefficient standpoint, the forward expanded hole performed poorly, presumably because of the increased interaction between the jet and the mainstream. Hyams et al. [6] studied the effects of slot jet shaping on the heat transfer downstream of a slot jet. They found that shaping of the slot inlet and exit provided significant gains in the film cooling performance. Also, Hyams and

* Corresponding author. Tel.: +1 407 823 5778.
E-mail address: kassab@mail.ucf.edu (A.J. Kassab).

1290-0729/$ – see front matter © 2009 Elsevier Masson SAS. All rights reserved.
doi:10.1016/j.ijthermalsci.2009.04.007

Nomenclature

BEM	boundary element method
CFD	computational fluid dynamics
CHT	conjugate heat transfer
C_p	specific heat at constant pressure
D	film cooling hole diameter
DNS	direct numerical simulation
f	an elliptic relaxation function
FEM	finite element method
I	momentum ratio, $I=(\rho V)_c^2/(\rho V)_{main}^2$
k	turbulent kinetic energy
L	film-cooling hole length
LES	large eddy simulation
M	blowing ratio, $M=(\rho V)_c/(\rho V)_{main}$
Pr	Prandtl number
Re_c	Reynolds number defined as $Re_c=\rho_c V_c D/\mu_c$
RKE	the realizable k–ϵ turbulence model
RSM	Reynolds stress model
SST	the shear stress transport k–ω turbulence model
T	temperature magnitude
V	velocity magnitude
V2F	the v^2–f turbulence model
$\overline{v^2}$	velocity variance scale
x	streamwise distance measured from hole centerline
y	vertical distance measured from top of the hole
z	spanwise distance measured from hole centerline
y^+	law of the wall coordinate
α	injection/inclination angle
ϵ	turbulent dissipation rate
η or Eta	local film cooling effectiveness
ρ	density
ω	specific dissipation rate

Subscripts

AW	adiabatic
c	coolant
Conj	conjugate
m	mainflow
r	recovery
t	total
∞	free stream

Leylek [7] examined the film cooling process for a shaped, streamwise injected, inclined jet for a blowing ratio of 1.25 and 1.88. Detailed field results as well as surface phenomena involving adiabatic film effectiveness and heat transfer coefficient are presented. They found that the laterally diffused, simple angle holes provided the best coverage and highest surface effectiveness magnitudes.

Wittig et al. [8], Thole et al. [9] and Gritsch et al. [10] studied the effect of film hole geometry on the film cooling flowfield. They provided measurements for the flowfield and the film cooling effectiveness downstream of a cylindrical, a laterally expanded, and a laterally forward expanded film-cooling hole. In these papers, the crossflow Mach number at the hole entrance side was taken up to 0.6, the crossflow Mach number at the hole exit side was taken up to 1.2, the blowing ratio taken up to 2, while the coolant-to-mainflow temperature ratio is kept constant at 0.54. In a companion paper, Giebert et al. [11] presented comparison of numerical calculations with flowfield measurements for the same hole geometries. Good results were achieved for the hole with forward-laterally expanded exit for the adiabatic film cooling effectiveness in terms of distribution of effectiveness along the jet centerline and its rate of lateral spreading. They noted that further improvements of the computational results may be possible if the computational grid is refined and a turbulence model which accounts for anisotropic effects is adopted.

Beger and Liburdy [12] presented distributions of velocity, streamwise vorticity, and other film cooling characteristics downstream of a single cylindrical hole, a single laterally diffused hole, and a single forward diffused hole. Kohli and Thole [13] numerically investigated the flowfield and in a diffused film cooling hole and its supply channel. Chen et al. [14] studied the compound-angle injection through a row of conical holes. Bell et al. [15] measured local and spatially averaged magnitudes of the adiabatic film cooling effectiveness downstream of five different hole geometries. Yu et al. [16] experimentally studied the effects of diffusion hole-geometry on overall film cooling performance.

For gas turbine applications, as in many other heat transfer applications, it is necessary to accompany the computation of the flow and associated heat transfer in the fluid with the heat conduction inside the adjacent solid surfaces, such as the case for the film cooling problem under consideration in this paper. The coupling of these two modes of heat transfer is termed as conjugate heat transfer (CHT). For a typical cooled turbine airfoil/shroud at operating conditions, there are three heat transfer problems linked together: external convection, internal convection, and conduction within the metal. The metal temperature distribution, and temperature gradients determine to a great extent component life. However, due to the complex, coupled nature of the heat transfer problem, accurate predictions of the metal temperature are difficult from a design standpoint. Generally, the approaches to calculate the

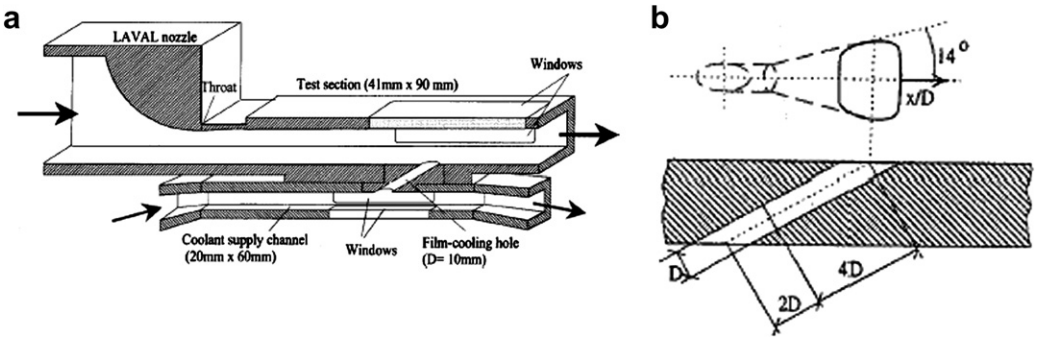

Fig. 1. Geometry of the experimental test case used in this study: (a) overall setup and (b) fan-shaped cooling hole details. From Gritsch et al. [10].

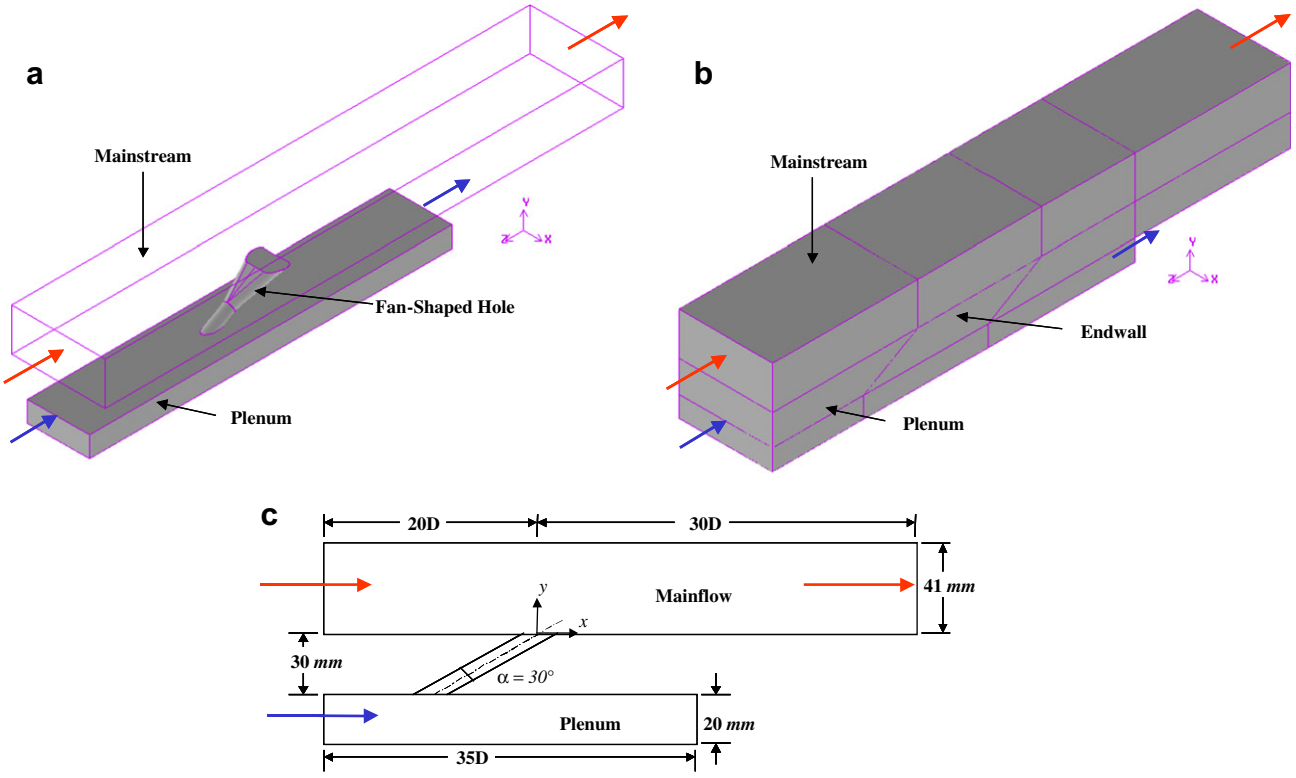

Fig. 2. Computational domain: (a) solid model of the adiabatic cases, (b) solid model of the conjugate case, and (c) schematic diagram.

conjugate heat transfer or the metal temperature can be divided up into two methods: the hybrid coupling procedure method and the homogeneous method. The hybrid method is performed using CFD solvers coupled to a conventional FEM or BEM solver to predict the temperature distribution at the metal walls. The main disadvantages of this method are problems associated with handling boundaries between different calculation areas. Whereas, the homogeneous method consists of direct coupling of the fluid zone and the solid zone using the same discretization and numerical approach. This makes it possible to have an interpolation-free crossing of the heat fluxes between the neighboring cell faces. Additionally, the wall surface temperature as well as the temperatures in the vane/endwalls is a direct result of this simulation.

One of the recent numerical studies by Bohn et al. [17] presented the calculations of a film-cooled duct wall imposed with adiabatic and a conjugate heat transfer condition for various configurations of cylindrical and shaped film-holes. They showed that the conjugate calculation method accounts for the significant influence of heat transfer on the velocity field within the cooling film. In particular, the secondary flow velocities are affected by local heat transfer, which varies significantly depending on the local position. Bohn and Kusterer [18,19] have investigated the 3-D cooling jet phenomena for blade leading edge ejection from non-lateral and radially inclined cooling holes.

Recently, Silieti et al. [20,21] investigated the numerical prediction of film cooling effectiveness in two and three dimensional gas turbine endwall/shroud for the cases of conjugate and adiabatic heat transfer models. They considered cooling slots, and cylindrical cooling holes at different blowing ratios. They incorporated the effect of different turbulence models in predicting the surface temperature and hence the film effectiveness. In the above studies, the turbulence closure was investigated using multiple turbulence models; the standard k–ϵ model (SKE), the RNG k–ϵ model, the realizable k–ϵ model (RKE), the standard k–ω model (SKW), the SST k–ω model, as well as the Reynolds Stress Model "RSM". In the two dimensional endwall study "film cooling slots", they found that the k–ϵ and RSM models yielded essentially the same results with slight deviations, whereas, the k–ω models underpredict the flow field in comparison with the other ones and overpredict the temperature field. For the three dimensional endwall study "cylindrical film cooling holes", they found that in the region for $(x/D \leq 6)$, the predictions of centerline film-cooling effectiveness by RKE model exhibited the best agreement with experimental data, whereas, the other four models under predicted the film-cooling effectiveness. Whereas, in the region for $(x/D > 6)$, all models over predicted the centerline film-cooling effectiveness and the best agreement was with SKE model and SKW model predicted the worst results. The k–ϵ models, especially RKE, perform better than the k–ω models in predicting the surface temperature distribution and hence, the film cooling effectiveness. Moreover, the results confirmed that the conjugate heat transfer models showed a significant difference in the temperature predictions in comparison with the adiabatic predictions.

Li and Kassab [22,23], Heidmann et al. [24] and Kassab et al. [25] pursued a different method of coupling the fluid and solid thermal problems. The basis for their technique is the boundary element method (BEM) for the solution of solid conduction problem. Since the thermal conduction in a solid is governed by Laplace equation for temperature, it may be solved only using boundary discretization. BEM takes advantage of this fact and does not require meshing of the solid volume.

This paper has three primary objectives: the first is to predict the film cooling effectiveness for adiabatic and conjugate heat transfer models in a 3D fan-shaped cooling holes. The second is to compare the results from these predictions to experiments. The third objective is the study effect of different grid topologies; i.e. hexahedral-, hybrid-, and tetrahedral-topology grid on the predicted film cooling effectiveness. The present study investigates the prediction of film cooling effectiveness from single, scaled-up fan-shaped hole geometry at an injection angle of 30°. The flow

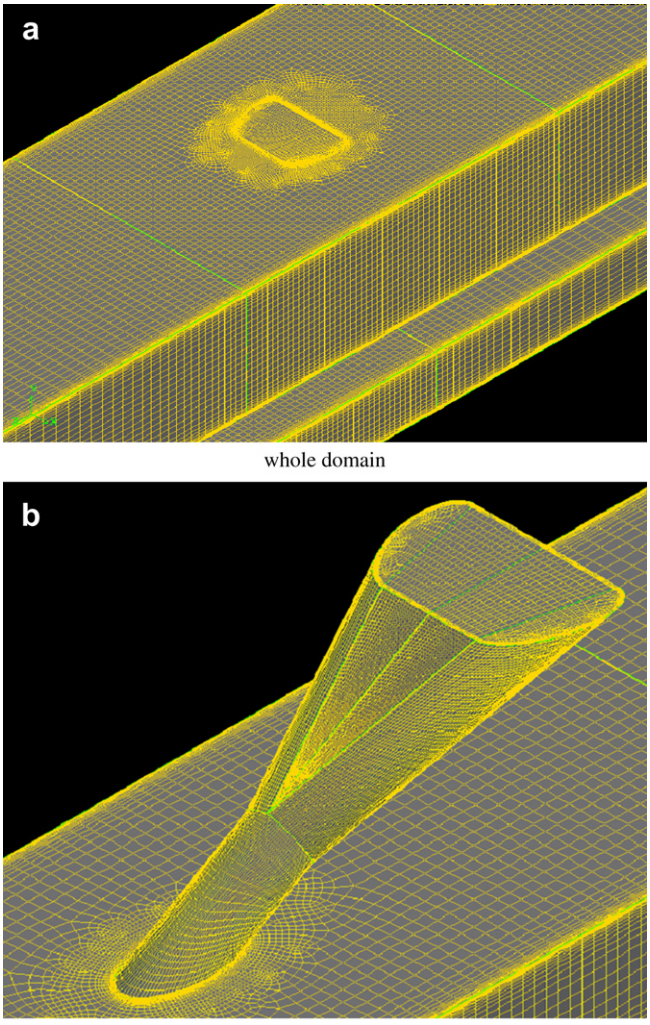

Fig. 3. Details of the grid used in the adiabatic case.

conditions considered are a blowing ratio of one, and the coolant-to-mainflow temperature ratio of 0.54. Turbulence closure was obtained using three different turbulence models: the realizable k–ϵ model (RKE), the shear stress transport k–ω model (SST) as well as v^2–f turbulence model (V2F). It also includes the velocity and temperature fields, in addition to centerline and two-dimensional film cooling effectiveness. Finally, the predicted centerline film cooling effectiveness has been compared to those reported in [10]. All the simulations reported in this paper were conducted using the commercial CFD code.

2. Validation test case: fan-shaped cooling-hole

We used the data reported in the open literature by Gritsch et al. [10]. A complete description of their experimental facility, located at the University of Karlsruhe, including the test section, and instrumentation used in acquiring the reported data, is given in [8,10]. They conducted a detailed measurements of adiabatic film cooling effectiveness for injection from single scaled-up film-cooling hole geometries. The geometries investigated included a cylindrical hole and two holes with a diffuser-shaped exit portion (i.e. a fan-shaped and a laid-back fan-shaped hole).

The film cooling test rig consisted of a primary loop representing the external (crossflow) flow and a secondary loop representing the internal (plenum) flow, see Fig. 1. In the primary loop, the test section is 90 mm in width and 41 mm in height. Whereas, the secondary channel has a cross-sectional area at the film cooling hole of 60 mm in width and 20 mm in height. The injection (inclination) angle of the film-cooling hole is ($\alpha = 30^\circ$) with a diameter of 10 mm, and length-to-diameter ratio of ($L/D = 6$).

The flow parameters investigated were typical for real film cooling applications. Each hole geometry was tested for a matrix of three internal (plenum) Mach numbers ($Ma_c = 0.0$, 0.3, 0.6) and three external (crossflow) Mach numbers ($Ma_c = 0.3$, 0.6, 1.2). The coolant supply passage internal Mach number of ($Ma_c = 0.0$) corresponds to the plenum condition.

3. Numerical methodology

We present the numerical methodology for this study. We first describe the geometry under consideration, and this is followed by the details of the three grid topologies developed to model the film cooling model and the imposed boundary conditions. Finally, we provide three turbulence models which are applied in computing film effectiveness for a variety of cases.

3.1. Geometry

The computational domain for the adiabatic cases matched the experimental test case. The solid models of the whole assembly are

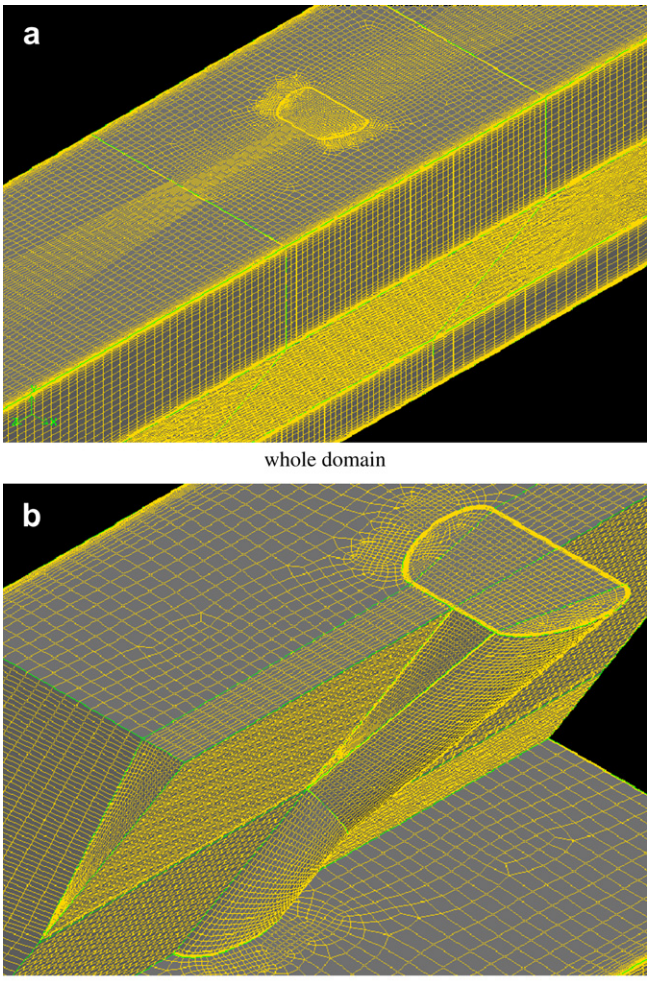

Fig. 4. Details of the grid used in the conjugate case.

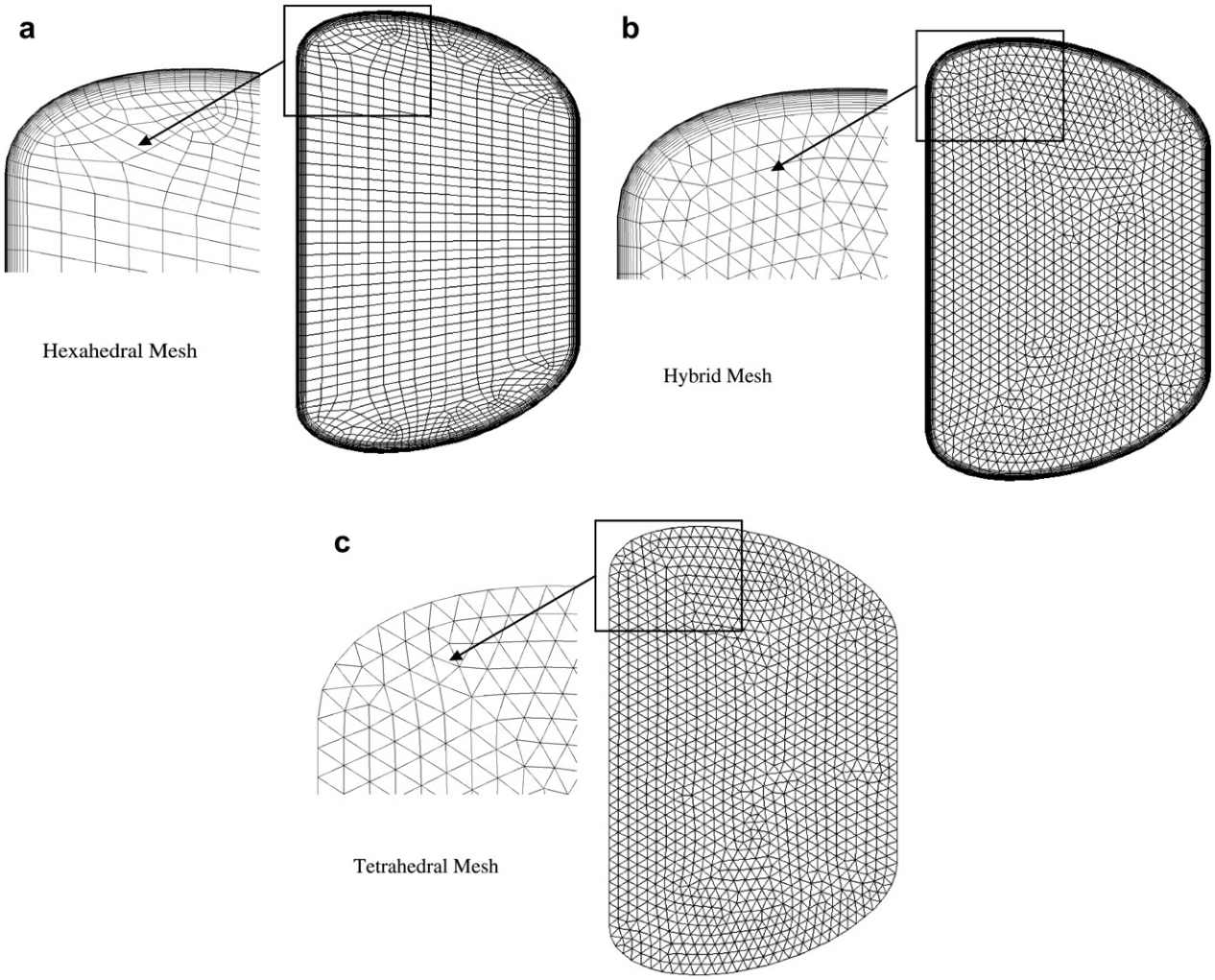

Fig. 5. Mesh details for the hexahedral-, hybrid-, and tetrahedral-topology grid in the cooling hole region.

shown in Fig. 2. For the adiabatic cases, the computational domain included the coolant supply channel (plenum), the fan-shaped cooling hole, and the main channel (cross hot flow). The crossflow test section was 90 mm in width and 41 mm in height, and plenum cross-section was 60 mm in width and 20 mm in height. The diameter of the film cooling hole was 10 mm with an injection angle of 30°. The metering section is 2*D* long, the lateral expansion is 14° resulting in a hole width of 30 mm at the hole exit, and the exit-to-entry area ratio is 3.0 (areas perpendicular to hole axis). The exit plane for the crossflow was located far downstream of the cooling hole at $x/D = 30$. The conjugate model was the same as the adiabatic model with an endwall/metal that has a cross-sectional area of 90 mm in width and 30 mm in height. Moreover, the width of the plenum had been adjusted to 90 mm.

3.2. Grid

A multi-block numerical grid was used in this study to allow the highest quality in all regions with the fewest number of cells. Multi-blocking refers to a technique in which the domain is partitioned into several different subsections in order to achieve the maximum control over the grid quality and density. Each section was then meshed using an appropriate topology. For this reason, the model was partitioned into 11 blocks for the adiabatic cases, and 20 blocks for the conjugate case. This allowed the use of a hexahedral mesh in all the blocks to achieve a high aspect ratio especially near the walls. The total number of computational cells are 1,867,168 for the adiabatic case and 2,375,139 for the conjugate case. The grid was created in using a commercial software. The cells in the near-wall layers were stretched away from the surfaces, and the first mesh point above the endwall is chosen such that the average y^+ is of the order of unity or less; i.e. first mesh point is in the range of (0.000001–0.000005 mm). A view of the computation grid for the adiabatic and conjugate cases is shown in Figs. 3 and 4, respectively. Since much effort was involved into meshing the fan-shaped hole with a hexahedral-topology grid (five blocks), this study is also concerned with different meshing schemes. For this reason, the fan-shaped hole has been meshed using a hybrid-topology grid and a tetrahedral topology grid. The hybrid grid consists of both prisms near the walls and tetrahedral cells; the total number of cells is 1,871,508. Whereas, the tetrahedral-topology grid consists only of tetrahedral cells with a total number of 1,476,141 cells, see Fig. 5. Grid independence was assessed by testing a finer mesh which resulted in a negligible change in the computed film cooling effectiveness downstream the film cooling hole.

3.3. Boundary conditions

The boundary conditions were chosen to match the experimental test case [10] as closely as possible. This study is carried out

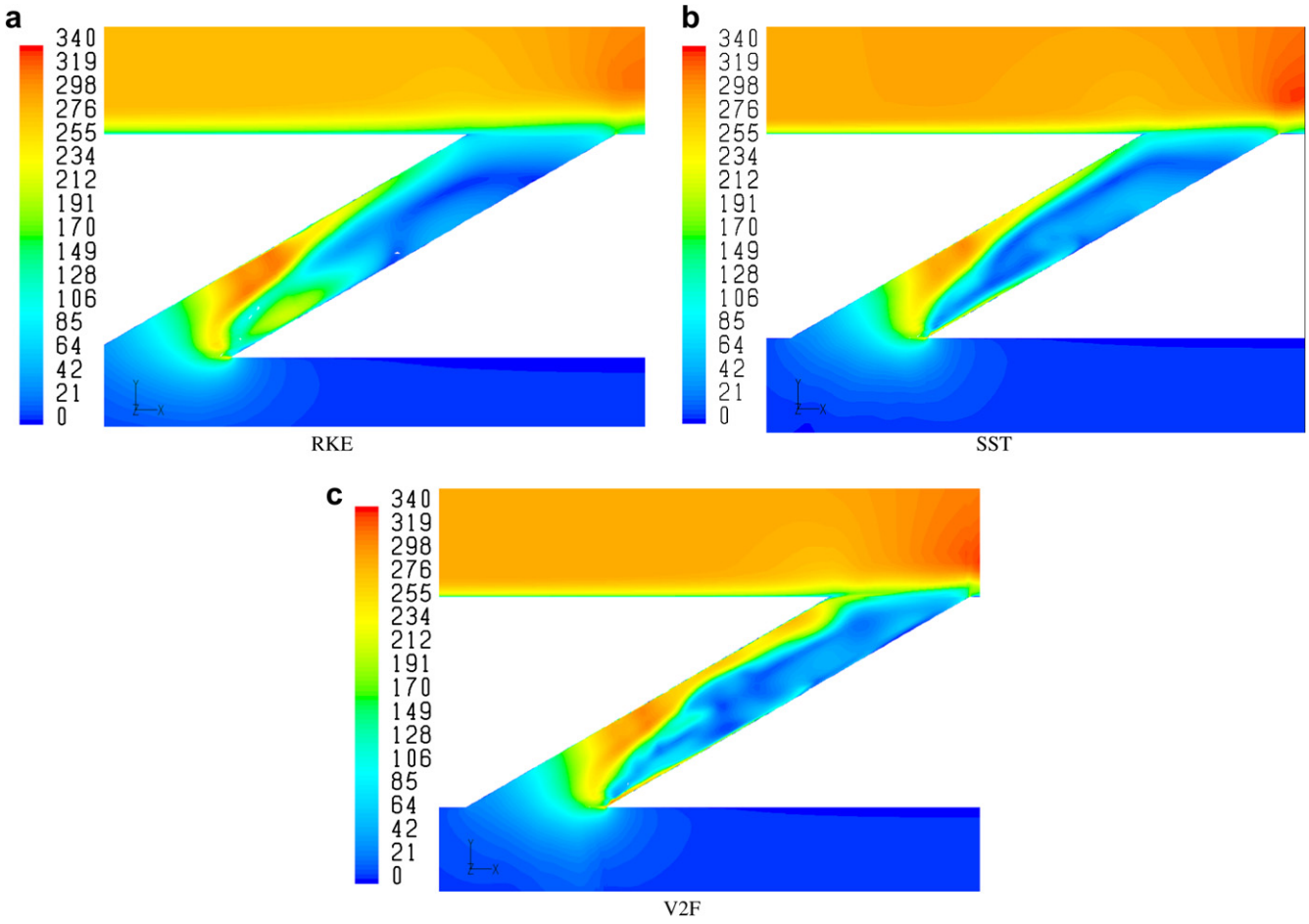

Fig. 6. Velocity magnitude contours (m/s) predicted by three turbulence models along centerline plane in the film cooling hole region with a hexahedral-topology grid.

for internal (plenum) Mach number of ($Ma_c = 0.0$) and external (crossflow) Mach number of ($Ma_c = 0.6$). Total pressure and total temperature are imposed at the channels inlet, and static pressure is imposed at the outlets. The total temperature at the primary channel (crossflow) inlet is 540 K, and 290 K at the secondary channel (plenum) inlet. Thus, the coolant-to-mainflow temperature ratio is 0.54, which can be assumed to be more representative for typical gas turbine applications. To achieve a blowing ratio of 1.0, the total pressure in the plenum was set to 109,750 Pa, whereas, the total pressure at the mainflow inlet is 100,400 Pa, and the static pressure at the outlet is 68,000 Pa. Inlet turbulence levels are set to 1.5% and 1% in the primary and secondary channels, respectively.

The fluid, air, was modeled as a compressible fluid using the ideal gas law, whereas, the other properties such as the specific heat ratio, thermal conductivity, and dynamic viscosity are piecewise-linear functions of temperature. For the conjugate heat transfer model, the endwall material was modeled as a high-temperature plastic material (TECAPEK) with a thermal conductivity of 0.2 W/mK for first case, and the second case it was modeled as AISI 347 stainless steel, with a density of 7978 kg/m^3. The thermal conductivity is piecewise-linear function of temperature.

3.4. Turbulence modeling

To investigate the effect of turbulence modeling on film cooling effectiveness predictions, turbulence closure was implemented using three different models: (1) the realizable k–ϵ model (RKE) of Shih [26] which resulted in a good agreement with the experimental data as shown for the case of cylindrical hole, (2) the SST k–ω model (SST) of Menter [27], and (3) v^2–f model (V2F) of Durbin [28]. These models were adopted in this study due to ease of implementation and computational economy, and due to the fact that they showed good agreement in predicted film effectiveness for the 2D slot cooling and single cylindrical film-cooling holes [28–30]. Alternative flow modeling such as DNS or models relying on subgrid turbulence models such as LES are not considered in this study because they are computationally very expensive and not suitable for practical industrial computations. The impact of each of the three turbulence models on the prediction of film cooling effectiveness is compared to experimental data [10] in the Results section below.

Briefly, the RKE model satisfies the so-called realizability constraints for the Reynolds stresses, specifically requiring positivity of the Reynolds stresses and satisfaction of Schwarz's inequality for the shear stresses. The RKE model has been shown by several researchers to reduce the excessive and non-physical production of turbulent kinetic energy characteristic of the standard k–ϵ model in areas of high irrotational strain.

The SST model differs from the standard k–ω model in two ways. First, the gradual change from the standard k–ω model in the inner region of the boundary layer to a high-Reynolds number version of the k–ϵ model in the outer part of the boundary layer. Second, the modified turbulent viscosity formulation to account for the transport effects of the principal turbulent shear stress.

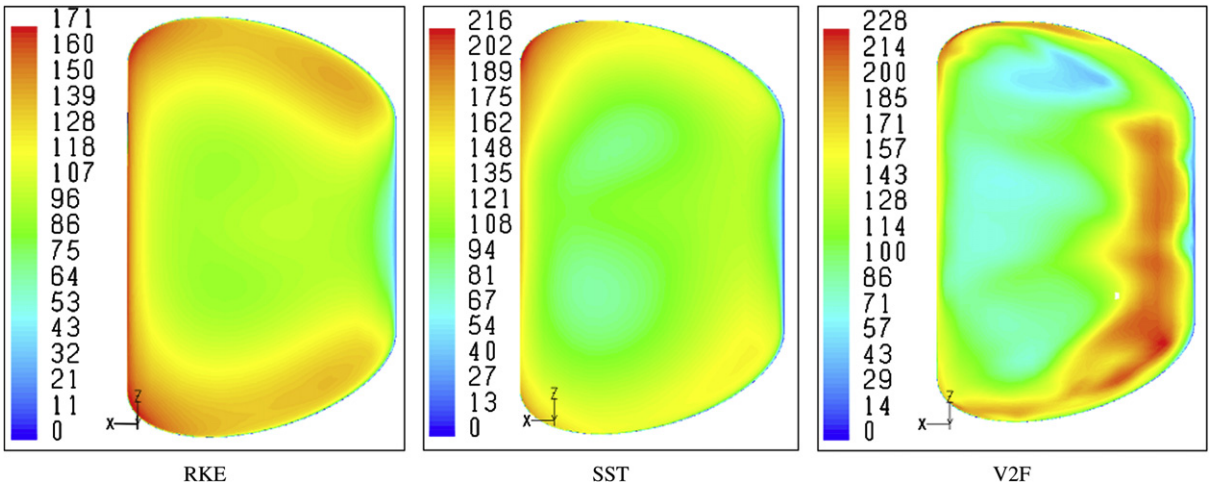

Fig. 7. Velocity magnitude contours (m/s) predicted by three turbulence models in the film hole exit plane with a hexahedral-topology grid.

Finally, the V2F model is an alternative to eddy-viscosity models and Reynolds Stress Model. This model is similar to the standard k–ϵ model, but incorporates the near-wall turbulence anisotropy and non-local pressure–strain effects. In fact, it is a general low Reynolds-number turbulence model that is valid all the way up to solid walls, and therefore does not rely on wall functions. Although the model was originally developed for attached or mildly separated boundary layers, it also accurately simulates flows dominated by separation. The V2F model is a four-equation model based on transport equations for the turbulence kinetic energy (k), its dissipation rate (ϵ), a velocity variance scale ($\overline{v^2}$), and an elliptic relaxation function (f). The distinguishing function of the v^2–f model is its use of the velocity scale ($\overline{v^2}$) instead of the turbulent kinetic energy (k) for evaluating the eddy viscosity (ϵ). The velocity variance scale ($\overline{v^2}$) which can be thought of as the velocity fluctuation normal to the streamlines, has shown to provide the right

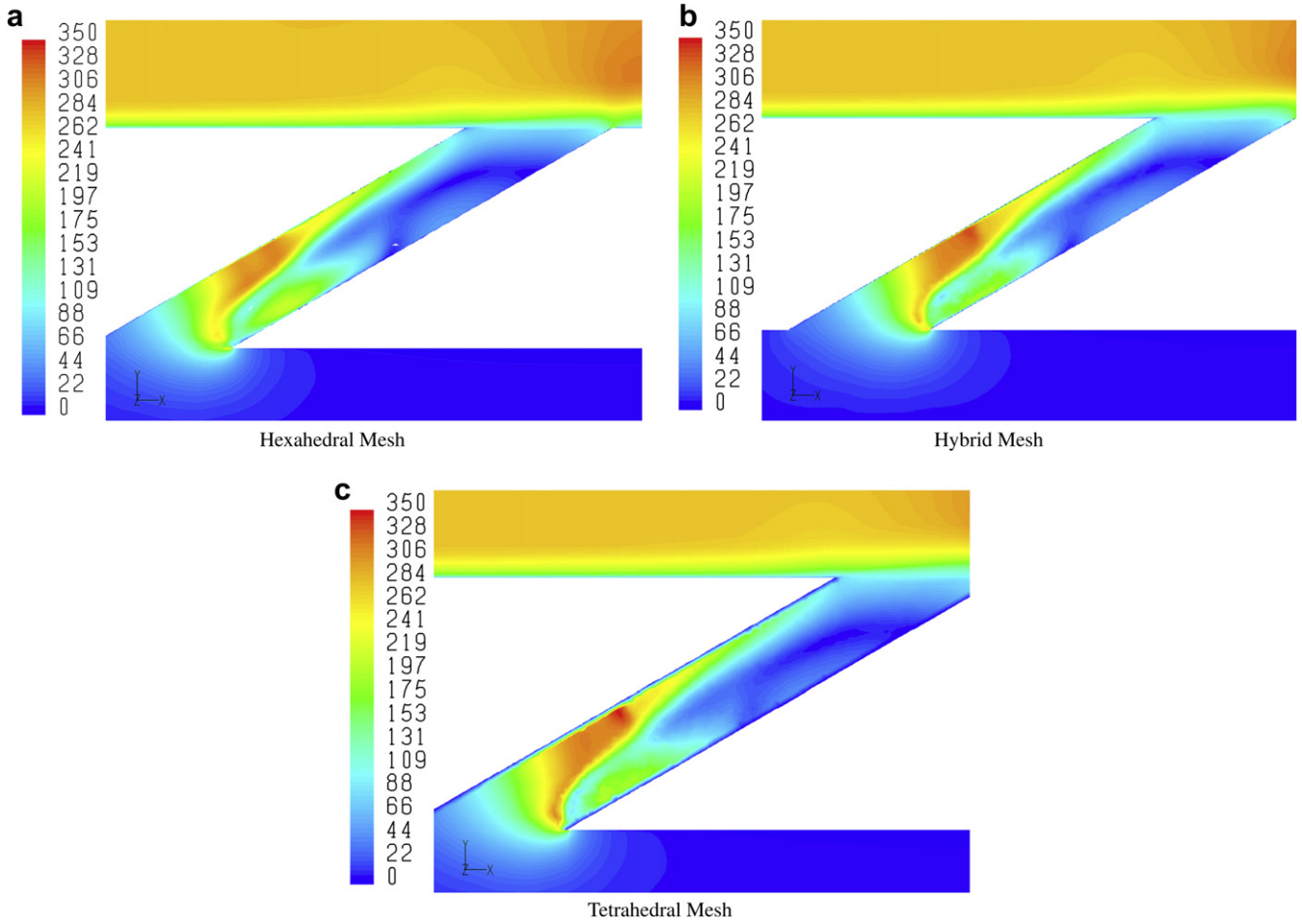

Fig. 8. Velocity magnitude contours (m/s) predicted by the RKE turbulence model along centerline plane in the film cooling hole region using three topology-grids.

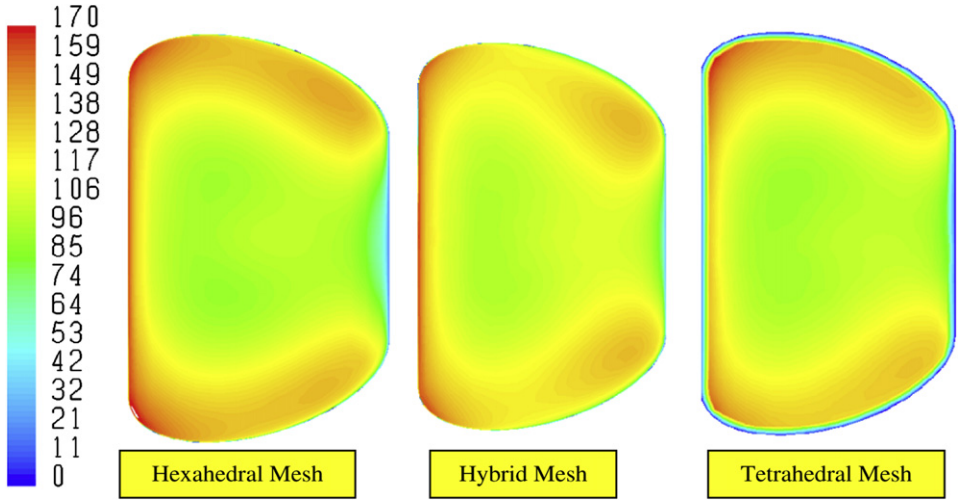

Fig. 9. Velocity magnitude contours (m/s) predicted by the RKE turbulence model in the film hole exit plane using three topology-grids.

scaling in representing the damping of turbulent transport close to the wall, a feature that k does not provide. Here, the v^2–f model uses an elliptic operator to compute a term analogous to the pressure strain correlation of the RSM. Ellipticity is characterized by a modified Helmholtz operator, which introduces wall effects via a linear differential equation.

4. Film cooling effectiveness

To define film cooling effectiveness, the surface temperature downstream of the cooling hole has to be measured. To be consistent with the experiment [10], the definition of the local film cooling effectiveness (η) was based on the mainflow recovery temperature as a reference temperature:

$$\eta(x/D, z/D) = \frac{T(x/D, z/D) - T_{r,m}}{T_{tc} - T_{r,m}} \quad (1)$$

here, $T(x/D, z/D)$ is the local temperature, and it is the adiabatic temperature for the adiabatic cases $T_{AW}(x/D, z/D)$, or the conjugate temperature for the conjugate case, $T_{Conj}(x/D, z/D)$. T_{tc} is the stagnation temperature of the coolant at the injection point, and $T_{r,m}$ is the recovery temperature of the mainflow, given by

$$T_r = T_\infty + (Pr)^{1/3} V_\infty^2 / 2C_p \quad (2)$$

In the experiment [10], the mainflow recovery temperature was measured on the test plate at a location not affected by the coolant ejection, for this reason, the recovery temperature was calculated at a location of $(x/D = -5)$.

5. Description of the flow solver

The simulations were processed using a commercial CFD code. The discretization used second-order upwinding with double precision accuracy. In the fluid zones, the steady, times-averaged

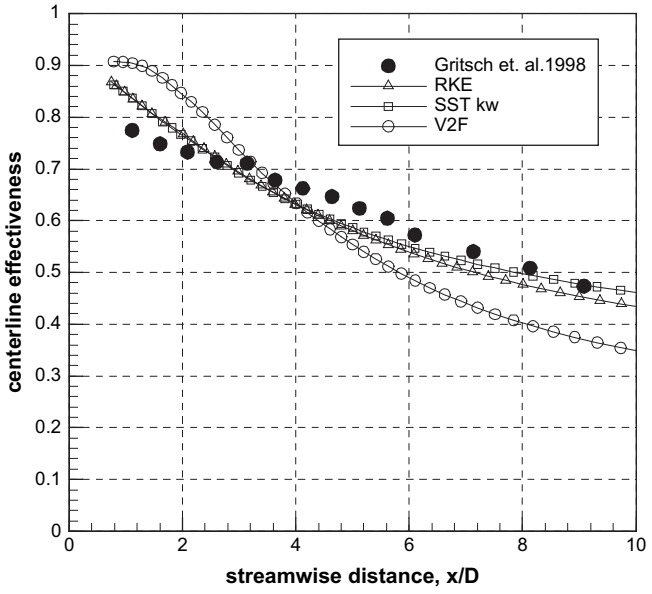

Fig. 10. Comparison of computed centerline adiabatic effectiveness (η) with data of Gritsch et al. [10] predicted by three turbulence models with a hexahedral-topology grid.

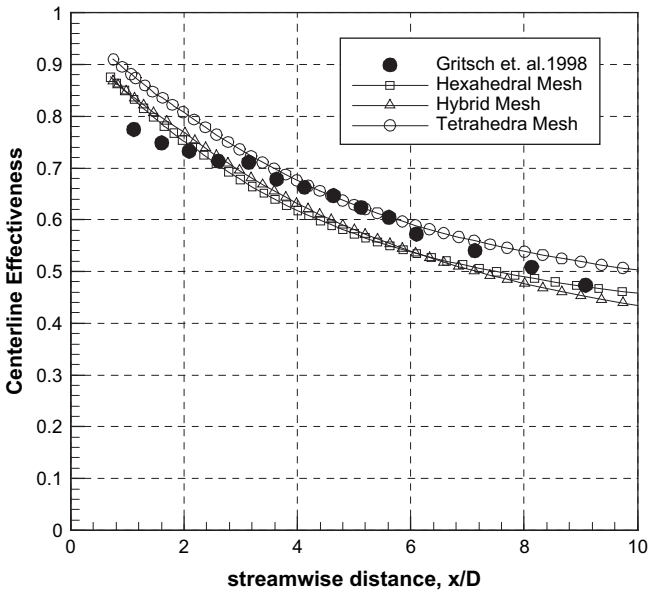

Fig. 11. Comparison of computed centerline adiabatic effectiveness (η) with data of Gritsch et al. [10] predicted by the RKE turbulence model using three topology-grids.

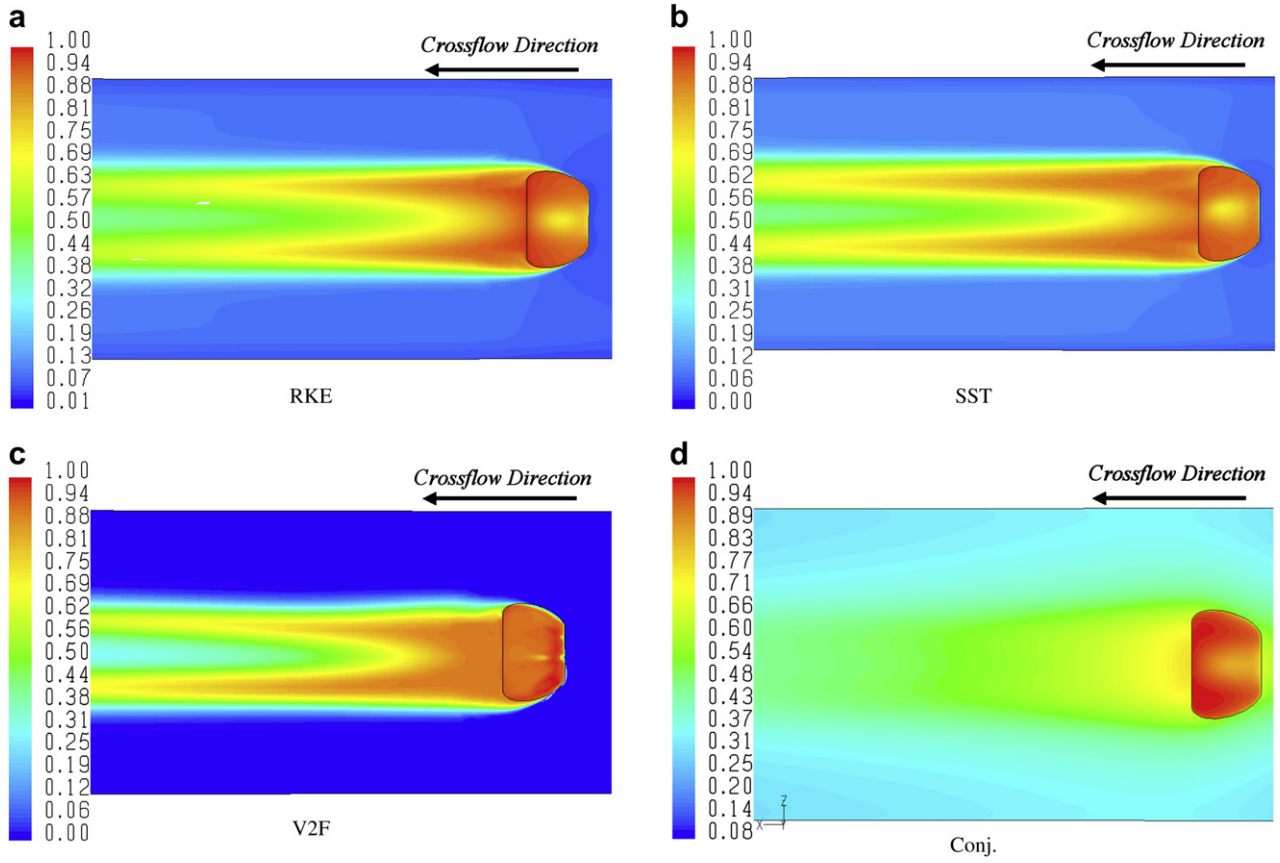

Fig. 12. Local adiabatic and conjugate effectiveness (η) predicted by three turbulence levels.

Navier–Stokes equations were solved, and pressure–velocity coupling was achieved with a pressure correction algorithm. In the solid zone, only the Fourier equation for heat diffusion was solved. At the fluid–solid interfaces, an energy balance was satisfied at each iteration, such that the heat flux at the wall on the fluid side was equal in magnitude and opposite in sign to the heat flux on the solid side. The temperature of the boundary itself was adjusted during each iteration to meet this condition.

Convergence was determined with the following criteria: (1) reduction of all residuals of at least four orders of magnitude, (2) global mass and energy imbalances dropped below 0.001%; and (3) the flow field was unchanging and the endwall surface temperature did not vary with additional iterations. Under these conditions, it was considered that a "steady state" had been achieved.

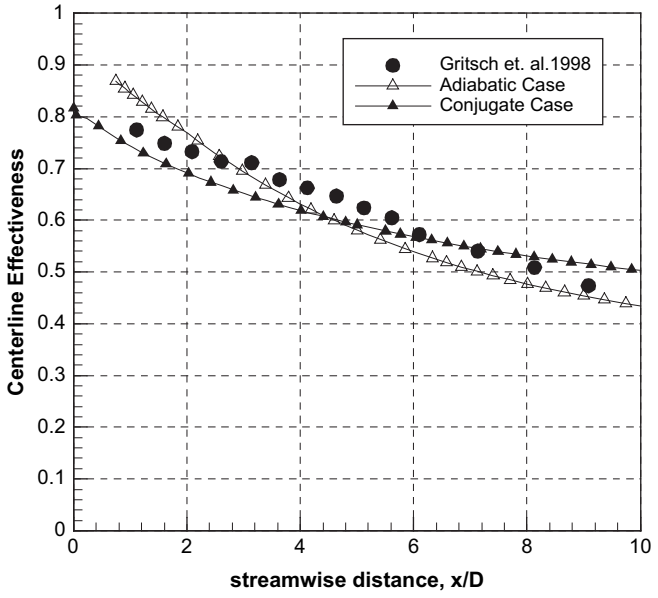

Fig. 13. Comparison of centerline adiabatic and conjugate effectiveness (η) with data of Gritsch et al. [10] predicted by the RKE turbulence model with a hexahedral-topology grid.

6. Results and discussion

This paper was primarily concerned with the computational prediction of adiabatic and conjugate effectiveness downstream of a 3D fan-shaped film cooling hole. Results were obtained for $L/D = 6.0$, blowing ratio of 1.0, and coolant-to-mainflow temperature ratio of 0.54 to match the experimental conditions [10]. First, results will discuss the adiabatic model cases for three different turbulence models and three grid topology schemes. Subsequently, the conjugate model cases predicted by the RKE turbulence model will be presented.

6.1. Velocity field results

Since the thermal field of a jet-in-crossflow interaction is dictated by the hydrodynamics, the flow field results were predicted by three turbulence models using a hexahedral mesh. In addition, the flow field results were predicted using three grid topologies: (1) hexahedral-, (2) hybrid-, and (3) tetrahedral-grids.

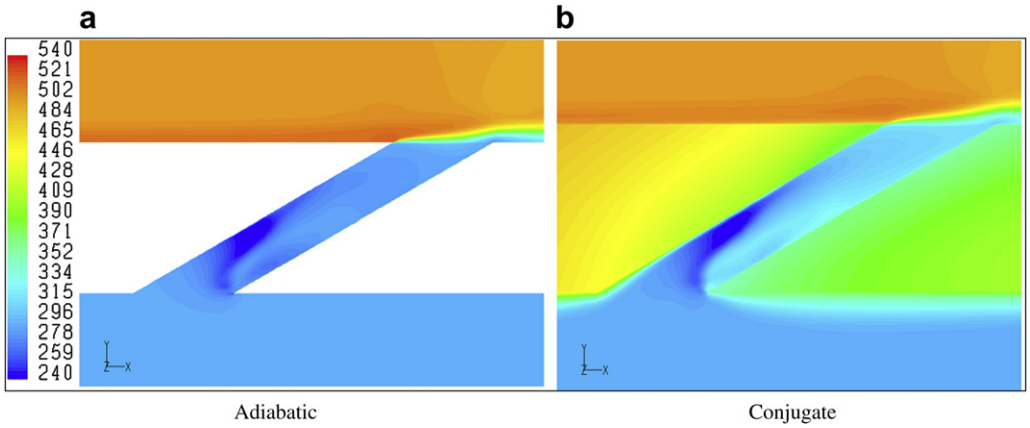

Fig. 14. Temperature magnitude contours (in Kelvin) along centerline plane in the film cooling hole region predicted by the RKE turbulence model with a hexahedral mesh.

When comparing grid topologies, the RKE turbulence model was used consistently.

The computed near-field velocity contours (m/s) along the centerline plane ($z = 0$) are shown in Fig. 6, where the turbulence closure was simulated using the three turbulence models. All models predict the low momentum region along the downstream edge and the corresponding high momentum or jetting region along the upstream edge within the film-cooling hole. However, it can be seen that the flow distribution is quite different from one turbulence model to next. This result is clearer in Fig. 7. For instance, V2F predicts a maximum velocity of 228 m/s, whereas RKE model predicts the maximum velocity to be 171 m/s. Moreover, the flow field predicted by the V2F is significantly different from the one predicted by RKE or SST. The flow distribution predicted by the SST model looks quite similar to the one predicted by the RKE model, especially at the film hole exit plane.

Figs. 8 and 9 show the velocity contours along the centerline plane in the film cooling hole region and at the cooling hole exit plane. Here, the results were predicted by the RKE turbulence model for the three different grid topologies: fully hexahedral grid, hybrid grid which was created from prisms near the walls and tetrahedral cells away from the walls, and fully tetrahedral grid. It can be seen that the flow field predicted for the case of a hybrid mesh is very similar to the case of a hexahedral mesh, whereas the tetrahedral case is very similar to the other cases in the flow core and quite different near the walls, which indicates the requirement to create a boundary layer near the walls in order to capture the high gradients of the flow field.

6.2. Film cooling effectiveness results

In this section, the local centerline and two-dimensional distribution of the film cooling effectiveness for the adiabatic and conjugate cases are reported and compared. Note that the streamwise distances are measured from the trailing edge ($x/D = 0$) of the film hole at the exit plane. Fig. 10 shows a comparison of computed centerline effectiveness with the data of Gritsch et al. [10] for the three turbulence models with a hexahedral mesh.

The blowing ratio for those cases is very close to one. It can be seen that all models overpredict the experimental data in the near hole region; i.e. ($x/D \leq 2$), whereas, RKE model and SST model predictions are very close to each other in this case (fan-shaped hole). On average, the predictions of RKE and SST models are very close to the experimental data. Surprisingly, the predictions of the V2F model are very different from the experimental data and the predictions of the other two models. The V2F model overpredicts the experimental data by up to 17% in the cooling hole immediate region ($x/D \leq 4$), and underpredicts the results by up to 27% in the intermediate region ($x/D > 4$). Overall, the RKE and SST models give better agreement with experimental data when compared to the V2F model. Fig. 11 shows the predicted film cooling effectiveness by the RKE model for three topology grids. It can be seen that the film effectiveness predicted with a hexahedral mesh is very similar to the case of a hybrid mesh, whereas, the results predicted with a tetrahedral mesh are higher than the other two cases. Surprisingly, the predicted film effectiveness with a tetrahedral mesh is in

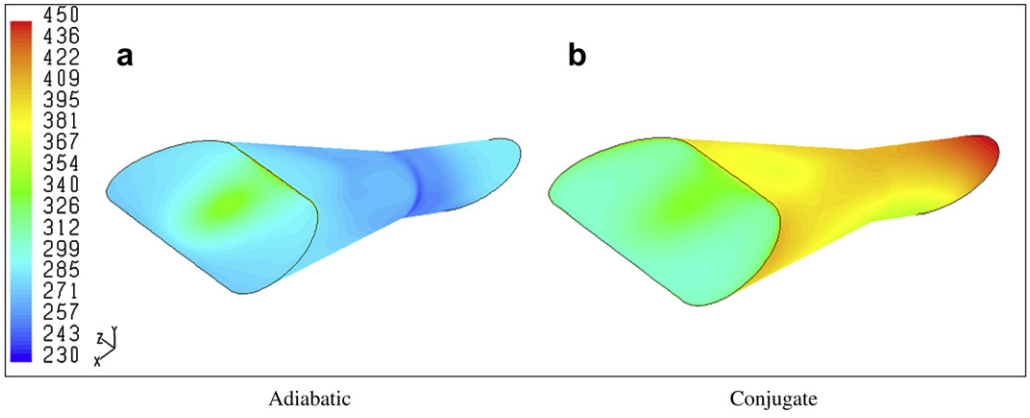

Fig. 15. Comparison of predicted surface temperature contours (in Kelvin) along film cooling hole predicted by the RKE turbulence model with a hexahedral mesh.

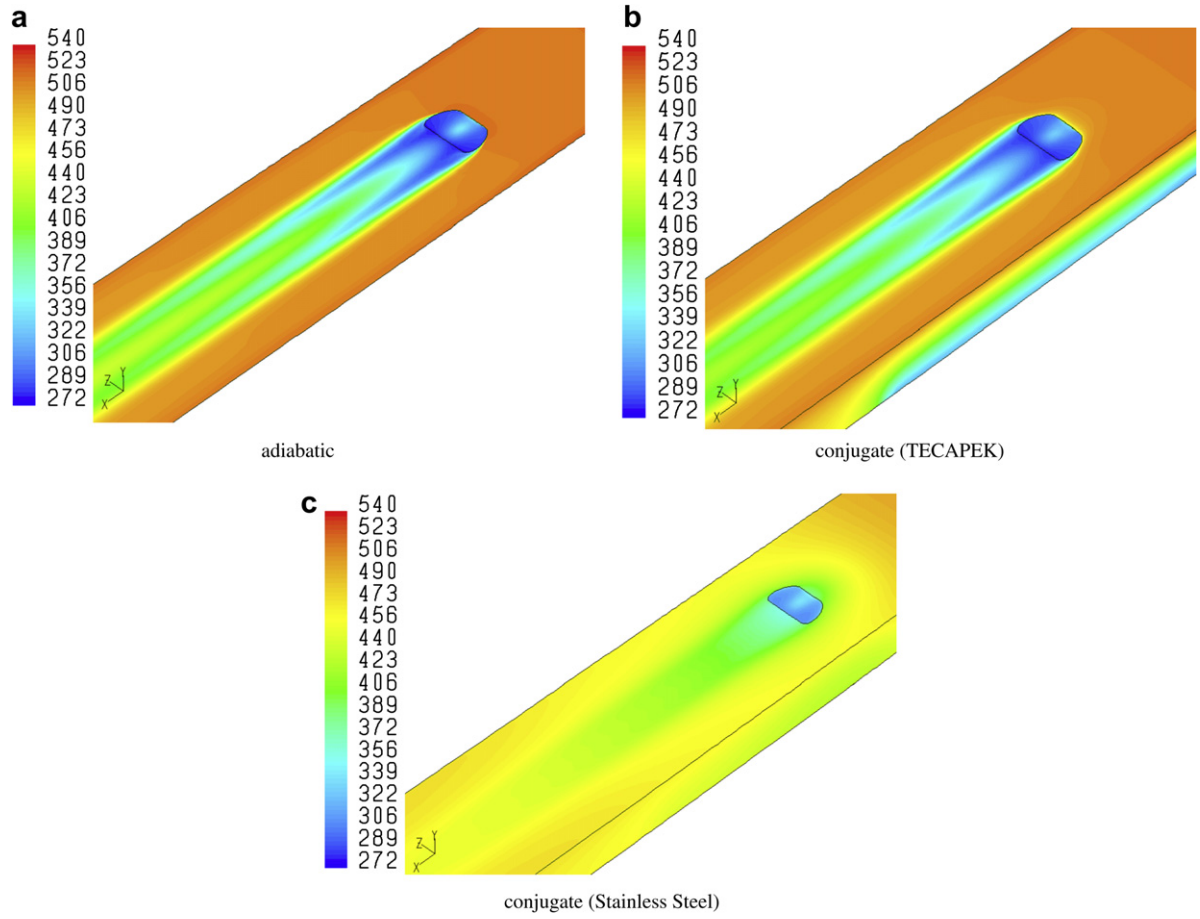

Fig. 16. Comparison of predicted surface temperature contours (in Kelvin) along the endwall in the film cooling hole region predicted by the RKE turbulence model with a hexahedral mesh.

a good agreement with experimental data, especially in the region of $(3 < x/D < 6)$.

Fig. 12 shows the two-dimensional distribution of the local film cooling effectiveness for the three adiabatic cases, as well as the TECAPEK conjugate case. The conjugate case was modeled with very low thermal conductivity (0.2 W/m K) using RKE turbulence model. This corresponds to a high temperature plastic material for the endwall (TECAPEK, the actual material used in the experiments of Gritsch et al. [10]). Qualitatively, all turbulence models tend to agree with the experiment [10], whereas, the distribution of the film cooling effectiveness for the conjugate case is significantly different.

The centerline effectiveness for the adiabatic and conjugate cases compared to the experiment is shown in Fig. 13. The predicted film effectiveness using the conjugate model is in a better agreement with the experimental data compared to the film effectiveness with the adiabatic model. This finding might be attributed to the fact that the experimental data has some conduction effects especially for this case; i.e. fan-shaped hole.

6.3. Temperature field results

This section presents the temperature distribution in Kelvin for the cases of adiabatic and conjugate heat transfer models. Since the RKE turbulence model gave good agreement with experimental data as shown in the film cooling effectiveness section, it had been used to predict the adiabatic and conjugate cases' results. Fig. 14 shows the computed near hole centerline temperature contours for the adiabatic and conjugate cases, respectively. For the conjugate case, the heat fluxes from the hot main flow into the wall heat-up the solid body. At the film cooling hole, an additional temperature increase of the cooling jet in comparison to the adiabatic case occurs because of the heat transfer from the hot wall into the cooling jet, see Fig. 15. An isometric view of temperature contours along the endwall and close to the cooling hole region is presented in Fig. 16 for the adiabatic and two conjugate cases, respectively. The conjugate cases were computed with very low thermal conductivity (0.2 W/m K). This corresponds to a high temperature plastic material for the endwall (TECAPEK, the actual material used in the experiments of Gritsch et al. [10]). The conjugate case was modeled using stainless steel properties for the endwall material. In the case of the fan-shaped hole, the results predicted from the adiabatic case are very similar to the results predicted by conjugate case with TECAPEK endwall material, whereas, this is not true for the cylindrical film cooling hole. These figures show clearly the differences in the temperature contours for both cases, which confirm that the conjugate heat transfer model can take into account the mutual influences of heat transfer on the fluid flow and vice versa.

7. Conclusions

In this paper, a comparative study is presented to study the ability of three turbulence models to predict the film cooling

effectiveness from a fan-shaped cooling hole: the realizable k–ϵ model, the SST k–ω model, and the v^2–f turbulence model. Three topology grids for the cooling hole were considered to test the effect of grid topology: hexahedral-, hybrid-, and tetrahedral-topology meshes. The boundary conditions were chosen in a way to be more representative for typical gas turbine applications and to match data reported in the open literature. The flow and temperature fields were discussed, in addition to local, two-dimensional distribution of film cooling effectiveness for the adiabatic and conjugate cases. Results were compared to experimental data in terms of centerline film cooling effectiveness downstream fan-shaped cooling hole. The predicted results using a hybrid mesh are identical to the ones predicted using a hexahedral mesh. This conclusion permits a significant reduction in the time required to generate the mesh, especially for fan-shaped holes. Surprisingly, the RKE model performs better than the V2F model in predicting the surface temperature distribution and, hence, the film cooling effectiveness. This result is in agreement with the results predicted in the authors' previous studies for cylindrical cooling holes. Also, the results confirm that conjugate heat transfer models predict a significant difference in the temperature predictions in comparison with the adiabatic models. This re-inforces the importance of considering the heat conduction the metal to accurately predict surface temperature. Results also show the effect of the conjugate heat transfer on the temperature field in the film cooling hole region, and the additional heating up of the cooling jet itself.

References

[1] R.J. Goldstein, Film cooling, Adv. Heat Transfer 7 (1971) 321–379.
[2] R.J. Goldstein, E.R.G. Eckert, F. Burggraf, Effects of hole geometry and density on three dimensional film cooling, Int. J. Heat Mass Transfer 17 (1974) 595–607.
[3] Y. Makki, G. Jakubowski, An experimental study of film cooling from diffused trapezoidal shaped holes, AIAA paper no. 86-1326, 1986.
[4] D. Schmidt, B. Sen, D. Bogard, Film cooling with compound angle holes: adiabatic effectiveness, ASME J. Turbomach. 118 (1996) 807–813.
[5] B. Sen, D. Schmidt, D. Bogard, Film cooling with compound angle holes: heat transfer, ASME J. Turbomach. 118 (1996) 800–806.
[6] D. Hyams, K. McGovern, J. Leylek, Effects of geometry on slot-jet film cooling performance, ASME paper no. 96-GT-187, 1996.
[7] D. Hyams, J.H. Leylek, A detailed analysis of film cooling physics: part iii – streamwise injection with shaped holes, ASME J. Turbomach. 122 (2000) 122–132.
[8] S. Wittig, A. Schulz, M. Gritsch, K. Thole, Transonic film-cooling investigations: effects of hole shape and orientations, ASME paper no. 96-GT-222, 1996.
[9] K.A. Thole, M. Gritsch, A. Schulz, S. Wittg, Effect of a crossflow at the entrance to a film-cooling hole, ASME J. Fluids Eng. 119 (1997) 533–540.
[10] M. Gritsch, A. Schulz, S. Wittig, Adiabatic wall effectiveness measurements of film cooling holes with expanded exits, ASME J. Turbomach. 120 (1998) 549–556.
[11] D. Giebert, M. Gritsch, A. Schulz, S. Wittig, Film-cooling from holes with expanded exits: a comparison of computational results with experiments, ASME paper no. 97-GT-163, 1997.
[12] P.A. Berger, J.A. Liburdy, A near-field investigation into the effects of geometry and compound angle on the flowfield of a row of film cooling holes, in: International Gas Turbine and Aeroengine Congress & Exhibition, Stockholm, ASME paper no. 98-GT-279, 1998.
[13] A. Kohli, K.A. Thole, Entrance effects on diffused film cooling holes, in: International Gas Turbine and Aeroengine Congress & Exhibition, Stockholm, ASME paper no. 98-GT-402, 1998.
[14] P.-H. Chen, D. Ai, S.-H. Lee, Effects of compound angle injection on flat-plate film cooling through a row of conical holes, ASME paper no. 99-GT-459, 1998.
[15] C.M. Bell, H. Hamakawa, P.M. Ligrani, Film cooling from shaped holes, ASME J. Heat Transfer 122 (2000) 224–232.
[16] Y. Yu, C.-H. Yen, T.I.-P. Shih, M.K. Chyu, S. Gogineni, Film cooling effectiveness and heat transfer coefficient distributions around diffusion shaped holes, ASME J. Heat Transfer 124 (2002) 820–827.
[17] D. Bohn, J. Ren, K. Kusterer, Conjugate heat transfer analysis for film cooling configurations with different hole geometries, ASME paper no. 2003-GT-38369, 2003.
[18] D. Bohn, K. Kusterer, Blowing ratio influence on jet mixing flow phenomena, AIAA paper no. GT-2002-30167, 1999.
[19] D. Bohn, K. Kusterer, Aerothermal investigations of mixing flow phenomena in case of radially inclined ejection holes at the leading edge, ASME J. Turbomach. 122 (2000) 334–339.
[20] M. Silieti, E. Divo, A.J. Kassab, The effect of conjugate heat transfer on film cooling effectiveness, ASME paper no. 2004-HT-FED-56234, 2004.
[21] M. Silieti, E. Divo, A.J. Kassab, Numerical investigation of adiabatic and conjugate film cooling effectiveness on a single cylindrical film cooling hole, ASME paper no. IMECE2004-62196, 2004.
[22] H.J. Li, A.J. Kassab, Numerical prediction of fluid flow and heat transfer in turbine blades with internal cooling, AIAA/ASME paper no. 94-1981, 1994.
[23] H.J. Li, A.J. Kassab, A coupled FVM/BEM solution to conjugate heat transfer in turbine blades, AIAA/ASME paper no. 94-1981, 1994.
[24] J.D. Heidmann, A.J. Kassab, E. Divo, F. Rodriguez, E. Steinthorsson, Conjugate heat transfer effects on a realistic film cooled turbine vane, ASME paper no. GT2003-38369, 2003.
[25] A.J. Kassab, E. Divo, J.D. Heidmann, E. Steinthorsson, F. Rodriguez, BEM/FVM conjugate heat transfer analysis of a three-dimensional film cooled turbine blade, Int. J. Numer. Methods Heat Transfer Fluid Flow 13 (5) (2003) 581–610.
[26] T.-H. Shih, W.W. Liou, A. Shabbir, Z. Yang, J. Zhu, A new k–ϵ eddy-viscosity model for high Reynolds number turbulent flows-model development and validation, Comput. Fluids 24 (3) (1995) 227–238.
[27] R. Menter, Two-equation eddy-viscosity turbulence models for engineering applications, AIAA J. 32 (8) (1994) 1598–1605.
[28] P.A. Durbin, Separated flow computations with k–ϵ–v^2 model, AIAA J. 33 (4) (1995) 659–664.
[29] S. Parneix, P.A. Durbin, M. Behnia, Computation of a 3d turbulent boundary layer using the V2F model, Flow Turbul. Combust. 10 (1998) 19–46.
[30] M. Behnia, S. Parneix, Y. Shabany, M. Behnia, Numerical study of turbulent heat transfer in confined and unconfined impingings jets, Int. J. Heat Fluid Flow 20 (1999) 1–9.